International Journal of Greenhouse Gas Control 84 (2019) 36–46

Contents lists available at ScienceDirect

International Journal of Greenhouse Gas Control

journal homepage: www.elsevier.com/locate/ijggc

Structural controls on the location and distribution of CO_2 emission at a natural CO_2 spring in Daylesford, Australia

Jennifer J Roberts[a,*], Aero Leplastrier[b], Andrew J Feitz[b], Zoe K Shipton[a], Andrew F Bell[c], Rūta Karolytė[c]

[a] Department of Civil and Environmental Engineering, University of Strathclyde, Glasgow, G1 1XJ, Scotland, UK
[b] Geoscience Australia, GPO Box 378, Canberra, ACT 2601, Australia
[c] School of Geosciences, University of Edinburgh, Grant Institute, Edinburgh, EH9 3FE, Scotland, UK

ARTICLE INFO

Keywords:
CO_2 flux
CO_2 storage
Mineral springs
CO_2 leakage
Natural analogues

ABSTRACT

Secure storage of CO_2 is imperative for carbon capture and storage technology, and relies on a thorough understanding of the mechanisms of CO_2 retention and leakage. Observations at CO_2 seeps around the world find that geological structures at a local and regional scale control the location, distribution and style of CO_2 emission. Bedrock-hosted natural CO_2 seepage is found in the Daylesford region in Victoria, Australia, where many natural springs contain high concentrations of dissolved CO_2. Within a few meters of the natural Tipperary Mineral Spring, small CO_2 bubble streams are emitted from bedrock into an ephemeral creek. We examine the relationship between structures in the exposed adjacent outcropping rocks and characteristics of CO_2 gas leakage in the stream, including CO_2 flux and the distribution of gas emissions. We find that degassing is clustered within ~1 m of a shale-sandstone geological contact. CO_2 emission points are localised along bedding and fracture planes, and concentrated where these features intersect. The bubble streams were intermittent, which posed difficulties in quantifying total emitted CO_2. Counterintuitively, the number of bubble streams and CO_2 flux was greatest from shale dominated rather than the sandstone dominated features, which forms the regional aquifer. Shallow processes must be increasing the shale permeability, thus influencing the CO_2 flow pathway and emission locations. CO_2 seepage is not limited to the pool; leakage was detected in subaerial rock exposures, at the intersection of bedding and orthogonal fractures.

These insights show the range of spatial scales of the geological features that control CO_2 flow. Microscale features and near surface processes can have significant effect on the style and location and rates of CO_2 leakage. The intermittency of the bubble streams highlights challenges around characterising and monitoring CO_2 stores where seepage is spatially and temporally variable. CCS monitoring programmes must therefore be informed by understanding of shallow crustal processes and not simply the processes and pathways governing CO_2 fluid flow at depth. Understanding how the CO_2 fluids leaked by deep pathways might be affected by shallow processes will inform the design of appropriate monitoring tools and monitoring locations.

1. Introduction

Carbon Capture and Storage (CCS) is an important component of CO_2 emission reduction strategies (OECD/IEA, 2015). Legislation and guidelines developed for CCS have set performance requirements to minimise leakage risk (Dixon et al., 2015). For CCS to be an effective mitigation strategy the injected CO_2 must remain securely in the subsurface (Schaffer et al., 2013). To avoid CO_2 leakage, site selection criteria must be guided by a thorough understanding of the geological characteristics that are most relevant to site integrity (Carpenter et al., 2011; Pearce and Czernichowski-Lauriol, 2004). As such there has been considerable research effort to understand the crustal fluid pathways of CO_2 migrating from depth (Holloway et al., 2007; Oldenburg and Lewicki, 2006; Roberts et al., 2017a). However there have been far fewer studies on fluid pathways in the near-surface. Effective surface monitoring strategies to detect and quantify CO_2 leakage from geologic stores therefore need to include an understanding of how near-surface processes affect leakage expression (Feitz et al., 2014; Jenkins et al., 2015; Roberts et al., 2017b).

Studies of natural analogues identify that geological structures, such as faults, govern CO_2 fluid flow on a macroscale (Dockrill and Shipton, 2010; Burnside et al., 2013; Miocic et al., 2016; Roberts et al., 2017a).

* Corresponding author.
E-mail address: jen.roberts@strath.ac.uk (J.J. Roberts).

https://doi.org/10.1016/j.ijggc.2019.03.003
Received 6 August 2018; Received in revised form 26 February 2019; Accepted 2 March 2019
1750-5836/

Fractures are also known to be an important control for fluid flow at meso- and micro-scale e.g. (Bond et al., 2013, 2017; Roberts et al., 2014), and the presence of fractures have complicated injection operations at pilot CCS sites (Rinaldi and Rutqvist, 2013; Verdon et al., 2013). To date, there has been little focus on the influence of microscale features, such as bedding planes and small fractures within foliated planes, on the surface expression of leaking CO_2—though these features are known to affect geofluid flow (Faulkner et al., 2010; Hippler, 1993; McCay et al., 2018). Further, field experiments designed to mimic CO_2 seepage by controlled CO_2 release at shallow depths have found CO_2 flow pathways are influenced by a number of local factors, and thus the location and style of seepage is difficult to predict (Roberts and Stalker, 2017). Thus, current understanding of the surface processes that govern CO_2 flow is limited. Here, we address this knowledge gap by presenting the characteristics of CO_2 leakage at Tipperary Mineral Spring, Daylesford (Victoria, Australia) where naturally occurring CO_2 seeps from exposed bedrock.

2. Geology and hydrology of the Daylesford region

The Daylesford region in the Central Highlands of Victoria hosts over sixty mineral springs that are naturally rich in dissolved CO_2 (Cartwright et al., 2000; Laing, 1977; Shugg, 1996; Wishart and Wishart, 1990). These waters have historically been of economic importance to the region, facilitating commercial water bottling operations, health spas, and tourism (Lawrence, 1969). Although the mineral springs were first described by European settlers in the 1830s (Wishart and Wishart, 1990), mining activities in the Victorian Gold Rush (1850s - 60 s) informed much of the current understanding of the geology and hydrology within the Daylesford area.

The regional geology comprises three principal units: deformed Ordovician turbidites of the Castlemaine Group, Devonian granites, and Quaternary basalts of the Newer Volcanics Province (VandenBerg, 1978) (Fig. 1). The turbidites consist of greenschist facies slates, shales, and sandstones in a 4500 m thick flysch sequence. These were extensively folded, fractured, and faulted in a single deformation event, the Tabberabberan Orogeny, estimated to have caused a 50–70% crustal shortening of this province (Cox et al., 1991a; Gray and Willman, 1991; VandenBerg, 1978; Gray et al., 1991). The timing of the orogeny is constrained by the coeval intrusion of granitoids, which date to the Late Devonian (Richards and Singleton, 1981). The regional structure is now dominated by NNW trending folds that extend up to 100 km in length with wavelengths between 10–15 km (Cox et al., 1991a; Gray and Willman, 1991; Lawrence, 1969; VandenBerg, 1978) (Fig. 1). Shorter subsidiary folds < 10 km length have wavelengths on the order of 150–500 m (Cox et al., 1991a). The compression also developed a series of west-dipping high-angle reverse faults across the region, with a minor set of east-dipping conjugates (Cox et al., 1991a; Gray and Willman, 1991; Shugg, 2009). Fold-associated fractures formed conduits for gold-bearing fluids during the late stages of regional deformation (Cox et al., 1991b). Mining of the Daylesford Gold Field between 1853–1951 and coincident underground mapping provided valuable insight into the subsurface structures (Maddicks and Butler, 1981). Mining records show west-dipping faults repeat at 60–120 m intervals in the Lower Ordovician sandstone-rich rocks near Daylesford (Shugg, 2009). Faults that cross-cut the metasediments contain fault breccia cemented with quartz (Shugg, 2009), and similar quartz-breccia 'reefs' are also found in anticline crests (Cox et al., 1991b). Reefs in the fold hinges and faults can extend for up to 4 km, and were the target for gold miners (Shugg, 2009). The Ordovician turbidites and Devonian granites are overlain by Newer Volcanic basalts, which form a widespread discontinuous plateau and date from 4.5 Ma to ~4.3 ka, with peak activity around 2.6 Ma (Gill, 1964; Mcdougall et al., 1966).

The faults, joints, fractures and cleavage developed in the bedrock facilitate groundwater and mineral water circulation (Shugg, 2009). The Ordovician turbidites and Quaternary basalts form regional fractured aquifers. The Ordovician bedrock has two distinct groundwater systems; a shallow fresh groundwater system and a second deeper mineral water system. The two systems mix to varying degrees, especially near the surface expressions of the mineral springs (Shugg, 2004). The CO_2 in the Daylesford Region mineral water is mantle-derived, and so has migrated from a deep-seated source into the Ordovician fractured aquifer (Cartwright et al., 2000; Lawrence, 1969). The mineral waters have a residence time of ~4.5 ka (Cartwright et al., 2002) and are assumed to recharge within the nearby Great Dividing Range, as well as through local volcanics that outcrop at higher elevations in the regional topography (Shugg, 1996).

The Daylesford mineral springs are high in calcium, magnesium, and bicarbonates, and so are quite different from typical Australian Na-Cl rich groundwater (Cartwright et al., 2002; Weaver et al., 2006). Individual spring water chemistry has changed little during 20 years of detailed measurements although some springs exhibit mixing with fresh water during discharge (Weaver et al., 2006). The total dissolved CO_2 content of the mineral waters is also consistent across the region (Cartwright et al., 2000; Laing, 1977; Weaver et al., 2006). Spring geochemistry is controlled by fluid-rock interactions facilitated by elevated CO_2 partial pressures (Karolytė et al., 2017), and, because each spring is geochemically unique (Laing, 1977), it is thought that the subsurface catchment feeding each spring is highly heterogeneous (Weaver et al., 2006).

2.1. The study area: Tipperary spring

The Tipperary Mineral Spring is one of 13 springs around the Daylesford township (Wishart and Wishart, 1990). Tipperary Mineral Springs Reserve is located 2.5 km west of Daylesford (37°20′14.8″S 144°07′14.2″E, Fig. 1). The spring eye is located on the west bank of Sailors Creek, beneath a footbridge crossing the creek, demarked by the presence of CO_2 gas bubbles into the creek bed. The bubbles are most apparent during the dry season when water level in the creek drops (Shugg and Brumley, 2003). A hand pump on the east side of Sailors Creek draws water from a borehole which was drilled in 2001. The bore encountered a significant flow of gassy mineral water in a highly fractured horizon at 45 m depth, and the borehole casing was pressure cemented in this portion (Shugg and Brumley, 2003). The mineral water is effervescent. Gases dissolved in the mineral waters of the Daylesford region are reported to range from 88.6 to 95.7 % CO_2 with between 0.4 – 0.8% O_2, 3.9–10.2 % N_2 and host trace quantities of He and Ne (Cartwright et al., 2000; Lawrence, 1969). The gasses emitted as bubbles at the seep bed are > 99% CO_2 (Karolyte et al., in prep). To date, the characteristics of the degassing, flux and distribution of CO_2 seepage at Tipperary have not been studied in detail.

3. Methods

Fieldwork at Tipperary was conducted in March 2017, towards the end of the summer when the creek level was low. The fieldwork aimed to collect geological and structural data at the site to observe the style of CO_2 degassing and measure gas fluxes.

High precision GPS measurements of bubble locations and outcrop/creek features were taken using an Altus APS3G high precision GNSS survey system for Real Time Kinematic (RTK) position measurements. A base station was set up at each locality and the Rover recorded the UTM coordinates of the feature. The positional accuracy of the RTK equipment is < 1 mm, but human error positioning the RTK will be on the order of < 1 cm. There were some time delays and complications obtaining position measurements due to tree cover and the footbridge which, in addition to the typically sporadic nature of the bubbles streams, meant that the location of the bubble streams was recorded using a local reference grid rather than the RTK. The bubble location error is therefore approximately ~10 cm.

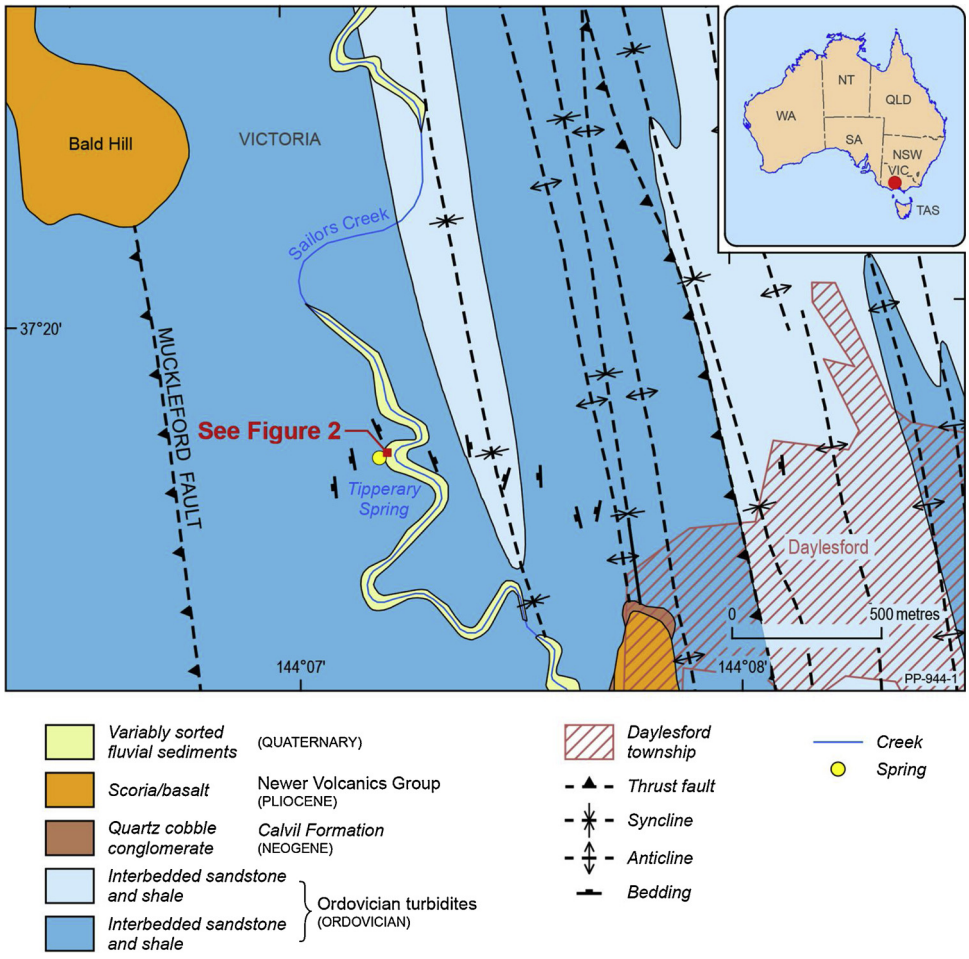

Fig. 1. Regional geological map, adapted from (Osborne et al., 2002), showing the main geological and structural features of the region north west of Daylesford, Victoria. The location of our study site, Tipperary Spring, is located along Sailors Creek. ***Inset***: Map of Australia, showing the location of Daylesford in red.

CO_2 flux measurements were obtained using a West Systems portable flux system with attached accumulation chamber (type B) and LI-840 A CO_2/H_2O gas analyser following the method established by Chiodini et al. (2001). A hollow 50 mm PVC pipe frame was attached to the base of the accumulation chamber as a floatation device in order to facilitate flux sampling at the water surface. The base of the accumulation chamber was therefore slightly submerged in water and this change in volume was accounted for when applying the ACK (a conversion factor between ppm/sec (instrument unit) and g/m^2/day). ACK temperature and pressure corrections (see Annex A) were made using meteorological measurements recorded at the nearby Ballarat Airport at 10 min intervals (Weatherzone, 2017). Where required, the floating flux chamber was attached to a pole to enable sampling of bubble streams without disturbing the creek sediments.

Flux measurements were made at bubbling points. Several readings were also taken at non-bubbling points across the pool to account for background diffuse degassing. The measurement period varied, but generally lasted for 90 s or longer, or until the accumulation in the chamber reached a CO_2 concentration of 20,000 ppm (at which point the accuracy of the gas analyser is negatively impacted). Time restraints prevented the quantitative measurement of every mapped bubble point, so our sampling focussed on the most vigorous and continuous bubbling points in the interests of producing the most reliable upper bound estimate of the total CO_2 emission rate. A more detailed discussion of the characteristics and style of the gas emissions at Tipperary is reported in Roberts et al (2018).

The presence of 'dry' seeps (CO_2 seepage from rock to atmosphere, not through water) was investigated using a tube connected to a Li-COR 81,000 A soil gas flux system ('CO_2 sniffer'), allowing CO_2 concentrations of the air to be continuously measured. The inflow tube was used to identify structural features in the outcrop that hosted dry gas seeps.

Structural measurements of outcropping bedrock were collected digitally using FieldMove Clino. The area of outcrop and the pool area were calculated from GPS measurements using ArcMap 10.2 ©ESRI 2013. Spatial statistical analyses were performed to quantitively examine seep distributions with respect to geological structures.

4. Results

4.1. Field observations

The low creek level in March 2017 meant that a series of isolated pools were found in the bed of Sailors Creek rather than a flowing stream. CO_2 degassing characterised by numerous bubble streams was observed in a single pool of water close to the footbridge near to Tipperary Mineral Spring (Fig. 2). The surface area of the pool was ~61.8 m^2 and water depth was greatest (40 cm) in the centre of the creek.

Two units of Ordovician rock crop out in the creek bed. The majority is fine-grained buff coloured massive sandstones that occur in 1–3 m thick beds, but a ~2.2 m thick blue-grey shale layer crops out beneath the footbridge. Rock bedding is oriented NW-SE and dips 65 - 80° to the NE (Fig. 3a,b). In contrast to the sandstone, the shale is thinly bedded (cm scale) with moderately well-developed bedding and parallel foliation. The shale is fissile, and more weathered than the sandstone and is less well exposed at the creek edge. The sandstone is much

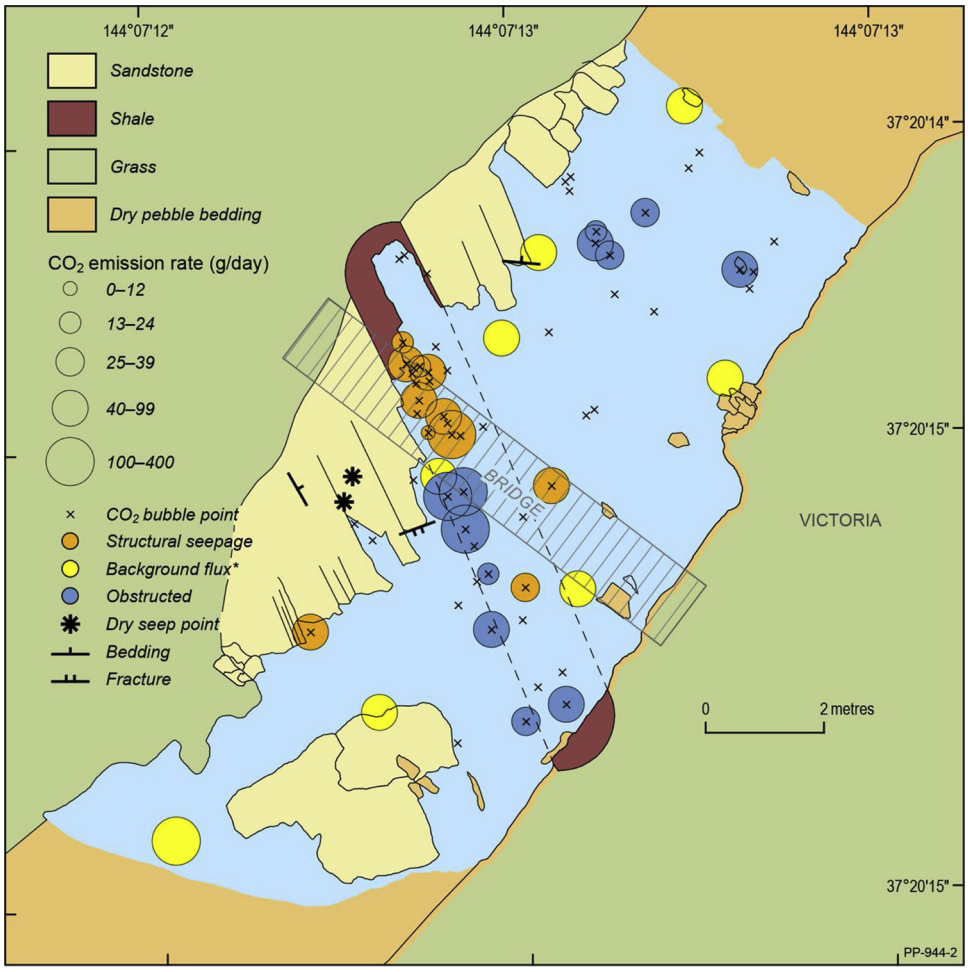

Fig. 2. Detailed map of the study area in Sailors Creek at Tipperary Springs Reserve showing the locations of CO_2 bubble streams (cross), and where measured, CO_2 seep rate depicted by the size of the halo (g/d). The colour of the halo represents whether the bubble visibly emerged from a structural feature (foliation, fracture or bedding plane; orange), or was not visible either because the seep point was obscured by river sediment or water depth (blue). In addition, background flux was measured at sites denoted by the yellow dots. Many of the bubble streams are positioned close to the lower contact between the sandstone and the shale. The principal bedding and fracture orientations are shown on the map. Two locations of focussed dry seepage were observed, where CO_2 emission was detected from the outcropping rock (asterisks). The river flows to the North East, but fieldwork was conducted in dry season when creek fill occurred as isolated pools (though CO_2 bubbling occurred in only one pool).

more cohesive, and while the fracture density is lower than in the shale, the fractures are longer. Three sets of fractures and joints are observed at the outcrop (Fig. 3a,c). The primary fracture set trends ~NE-SW and dip steeply to the SE. These vary between ~10 - 50 cm spacing, and fractures in the sandstones extend through the shale. At least two exposed fractures in the sandstone show evidence of vuggy quartz mineralisation. In the shale, the NE-SW fractures are closer spaced (~10 cm) but shorter; often terminating before the sandstone. A second set of shallow-dipping fractures trend ~NW-SE; these are mostly restricted to the sandstone unit, some are mineralised with quartz, several are non-planar or are not laterally pervasive. There is no visible offset along this fracture set, thus they could classify as joints. A final minor set of near vertical fractures trend E–W. These are poorly developed, only centimetres in length, with large (~1 m) spacing and no clear evidence of mineralisation at the outcrop.

4.2. CO_2 seepage from submerged rock in Tipperary pool

Fig. 2 shows the locations of CO_2 bubble streams in Tipperary pool. The activity of the bubble streams varied in regards to how long they

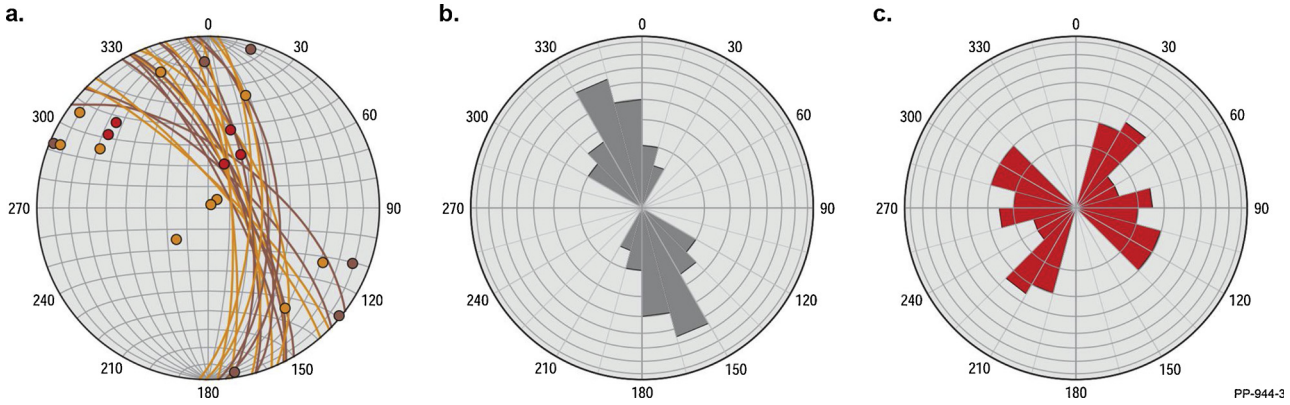

Fig. 3. Structural data from outcropping Ordovician turbidites of the Castlemaine Formation in the river bed at Tipperary Spring showing (a) Stereonet of bedding and bedding-parallel cleavage plotted as great circles, and poles to open fracture planes and poles to veins (where sandstones, orange; shales, brown; veins, red); (b) rose diagram of bedding and (c) fracture orientation, including open fractures and veins (shallow dipping fractures will be under-sampled). Structural data was analysed using Orient software (Vollmer, 2015).

were active (bubbles emitted) and inactive (no bubbles emitted). Some were extremely intermittent, with many minutes, sometimes half an hour before another bubble exhalation, and the bubble streams short lived. Others lasted many seconds, and were comprised of a continuous exhalation of small bubbles. More persistent seeps could bubble for up to seven minutes and were only interrupted with brief pauses. In total, 60 underwater degassing points (bubble streams) were identified and mapped within Tipperary pool, and CO_2 fluxes were measured at 24 (40%) of the locations.

75% of the bubble streams with measured fluxes were located in the shale, and preferentially towards the contact between the shale and the sandstone. CO_2 bubbles emerged along submerged foliation planes within the shale, along bedding planes of the sandstone or at the intersection between the foliation and open fractures or bedding and fractures. 46% (11/24) of the bubble streams with measured fluxes emerged from small fissures offered by dilated foliation or bedding planes, and nearly half of these occurred where open fractures or joints intersect the foliation or bedding plane. The origins of the remaining 13 bubble streams were obscured; either by sediment or because it was not possible to see to the bottom of the pool as the water was quite turbid (due to ferruginous flocculate and algae), a common feature of many of the mineral springs (Shugg and Brumley, 2003).

Background diffuse degassing rate was measured at eight (non-bubbling) locations across Tipperary pool and ranged from 49.4 – 229 g m^2 d^{-1} (mean 79.2 g m^2 d^{-1}). These values were relatively high compared with emissions at other spring-fed pools in the Daylesford region (Roberts et al., 2019), and suggests that the dissolved CO_2 content of the pool water is high, but also variable across the pool, but no water samples were collected to verify this. The minimum daily emission rate for the pool was estimated by applying the average of the background readings across the surface area of the pool and neglecting the input of bubbling points giving a value of ~4900 g d^{-1}. Degassing rates at bubbling points ranged from 11.4 to 374 g d^{-1}. These values will represent combined emission of CO_2 from bubbles and water surface degassing. Bubbling rates were greatest at the sandstone-shale contact beneath the footbridge (Fig. 2). The maximum daily emission rate from the pool was calculated by assuming that bubbling from the point sources was continuous and adding the sum of the maximum measured bubble point emissions (2267 g d^{-1}) to the maximum background degassing rate giving a value of 7170 g d^{-1}. Yearly emissions from the pool can therefore be constrained within the lower and upper estimates of 1.8–2.6 t y^{-1}, which correspond to average flux rates across the pool area of 79 - 116 g m^2 d^{-1}.

4.3. CO_2 seepage from outcropping rocks

The CO_2 sniffer detected two locations where atmospheric CO_2 concentrations were up to 6000 ppm in the dry outcrops on the banks of the creek. In both cases the high CO_2 concentrations were extremely localised, and occurred in jogs or intersections in uncemented, bedding-orthogonal, fractures in sandstones (Fig. 4a,c). Further, these concentrations were consistently high. That is, returning to the same location several minutes later, similarly high concentrations from between 2000 to 6000 ppm were recorded. Consistently high CO_2 concentrations at these features suggests that seepage was continuous during the survey period (several hours), and also rules out the possibility that elevated CO_2 concentrations were an artefact caused by density-driven pooling of CO_2 degassed from the pool at times of particularly low wind speed. Interestingly, when we poured ~1 L water over the seeping fracture the CO_2 concentration returned to background atmospheric levels and took 14 min for CO_2 seepage to become re-established. Weak elevations in CO_2 concentration (up to 500 ppm) were detected along a bedding-orthogonal fracture in the foliated shale (Fig. 4b,d). However, the area of shale outcrop was less than the sandstone (in part due to bedding thickness, in part due to the morphology of the outcrop) and so we cannot compare instances of CO_2 detection per area of rock.

4.4. Spatial distribution of seepage

We use a two-point spatial correlation function (TPCF) to quantitatively investigate the alignment of mapped CO_2 bubble streams with geological structures at Tipperary. The TPCF quantifies the departure from homogeneity of a distribution of points, and the distribution of azimuths between all point pairs can be measured to examine anisotropy in the point distribution. The correlation function is expressed as the probability of finding a pair of points within incremental radius and azimuth. For an ideal scenario with no finite size effects the correlation function will plot as a power law, $P \propto r^{\kappa}$, where P is probability, r is radius, and the constant κ describes the spatial distribution of points. For randomly distributed points, $\kappa = 2$. If points are clustered, $\kappa < 2$. For points that are distributed on a line, $\kappa = 1$. Other arrangements, such as points distributed on multiple lines, will give κ values between 1 and 2.

The study area is spatially limited; the pond is asymmetric and approximates a 11 x 5 m rectangle. As such, synthetic data was created to act as a 'control' for comparison with the CO_2 bubble stream distributions. The total numbers of measured and synthetic points are the same (60). Synthetic data were generated from multiple random (Poisson) point distributions for different spatial scenarios, including an 11 x 11 m exposure and an 11 x 5 m exposure with long axis orientated NNE, mimicking Tipperary pool which is only 4.4 m at its narrowest point and longer in the NE-SW orientation (see Fig. 2). Additional synthetic data were generated for different spatial scenarios, outlined in Table inset Fig. 5, including Poisson distribution along a line (orientated 330° within a 10 x 5 m exposure, long axis NNE), or within a given distance of a line, to explore which distribution best describes the observed data.

TPCF results, shown in Fig. 5, are presented for the bubble points and for synthetic scenarios. The roll-off at distances > 4 m is a finite size (censoring) effect caused by the spatial extent of the outcrop (e.g. Bonnet et al., 2001). For the synthetic data, κ is affected by the dimensions of the study area (outcrop/pool); for scenario B, random points in a 10 m square, κ is close to 2 (random) whereas for scenario C, κ is ~1.75. Since κ values < 2 indicate clustering of point data, even for Poisson data, this is a finite-size (censoring) effect caused by the spatial extent of the outcrop creating an artificial alignment amongst point data. Reducing the width of the rectangle reduces the κ value, until the extreme case, scenario D, where points are distributed on a line, when $\kappa = 1$. For bubble data, κ = ~1.5. This TPCF pattern is best modelled by scenario E, where the width of rectangle is thinner than the shale outcrop.

Point pair azimuths at different point separation distances are shown in Fig. 5 for bubble point (scenario A) and synthetic (scenarios B–E) data. More point pairs are located at shorter distances in the bubble data than in the synthetic data; there are over twice as many bubble point pairs within less than 1 m of each other than for the synthetic data C (164:75). Since the total number of points in the datasets are the same, these differences illustrate that the bubble points are more clustered than in all synthetic datasets.

At point separation distances above 2 m the finite size effect caused by the orientation of the study area clearly influences the point pair azimuths. In scenario C the rectangle is orientated NNE like the Tipperary pool, whereas other synthetic scenarios are orientated NW, like the bedding at Tipperary. The > 2 m point pair azimuths in these synthetic scenarios clearly reflect the orientation of the rectangle long axis (Fig. 5iv). The effect of the orientation of Tipperary pool is evident in the bubble point pair azimuths, as is the control of the NNW trending bedding/foliation 5 A(iv). The control of bedding/foliation on bubble pair azimuths continues to be visible at point pair distances below 2 m 5 A(ii,iii); 38% (63 pairs) of bubbles located within < 1 m of each other, and 51% of bubbles located between 1–2 m of each other exhibit

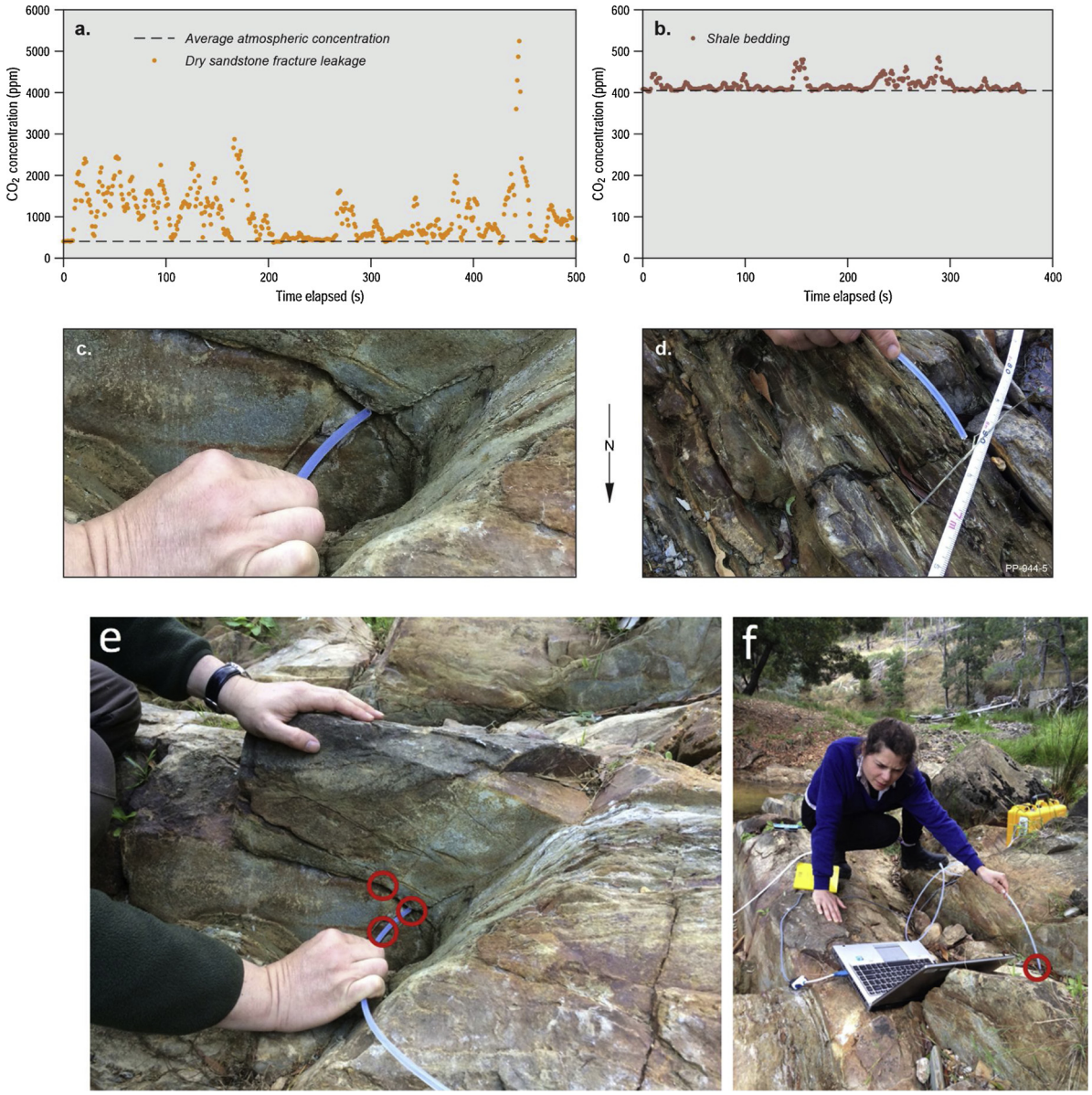

Fig. 4. (a) CO_2 concentration data recorded every second by the 'CO_2 sniffer' (a LI−COR 81,000 A soil gas flux system) when the inflow tube was positioned (a) around a fracture intersection in a sandstone bed (orange) and (b) across shale units (red). Concentration spikes in (a) and (b) indicate where the sniffer passed over points of very localised degassing, and the concentration then varies as the tube is moved along the features, or back and forth over points of high concentration. (c) Photograph of a sandstone bedding surface intersected by two fractures. High CO_2 concentrations shown in (a) were detected at this fracture intersection and at two jogs, detailed in (e). (d) Photograph of a fracture cutting the foliated shale unit. Peaks in CO_2 concentration along this fracture were much lower, as shown in (b). Photographs (e) and (f) show the specific points of CO_2 degassing from the sandstone.

a NNW-SSE (315°–360°) orientation. In contrast, since synthetic data are all randomly distributed in a given space, the dimensions of the study area are not visible in the point pair azimuths at distances < 2 m (except for scenario D, where point pair azimuths are the same at all separation distances).

While bubbling points were observed in the field to be located along bedding, foliation and fracture planes, the point azimuths < 2 m do not exhibit very clear spatial trends other than the bedding and foliation. At Tipperary, a range of fracture orientations were measured (see Fig. 3c) with dominant sets trending NE-SE and NW-SE. Bubble pairs do show peaks in these orientations at < 2 m separation, but it is difficult to distinguish these from noise.

5. Discussion

5.1. The role of geological structures and CO_2 seepage at Tipperary

Central Victorian mineral water springs are commonly channelled by regional thrust faults and can emerge close to anticline crests (Shugg, 2009). Although obscured in the field area, the regional geological map shows an inferred NNW-SSE trending anticline to the West of Sailors Creek, its projected axis passing less than 20 m from the creek. An inferred NW-SE fault runs in the same orientation as the creek but is mapped as terminating before intersecting the creek (Fig. 1). In 1912 the Daylesford Borough Engineer developed a cement-lined pit approximately 50 m SW of the current location of CO_2 degassing. This pit is now in disrepair, but was built to channel the spring waters, for ease of access to the mineral spring. The engineer's sketches of the area around the pit record a NE-SW trending fault and a NNW-SSE trending

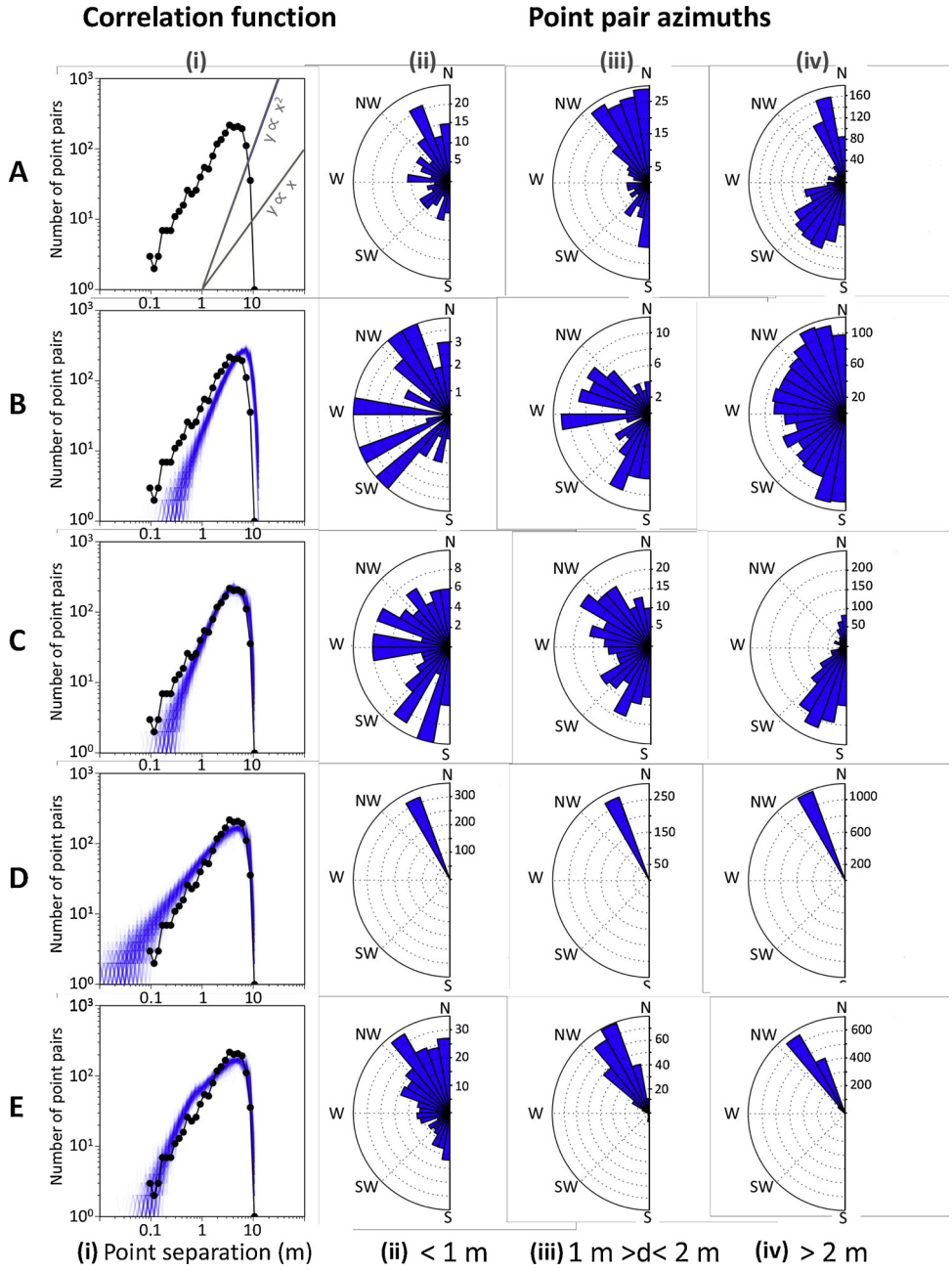

Fig. 5. (i) Point-distance correlation functions for observed seep pairs (black) and synthetic point simulations (blue) for scenarios A to E. Polar plots show the azimuths and number of point pairs with separation distances (ii) below 1 m; (iii) greater than or equal to 1 m but less than 2 m; and (iv) greater than or equal to 2 m but less than 10 m. Roll-off in the TPCF occurs at ~4 m separation distance due to the outcrop extent. **Table inset:** Summary of the different spatial scenarios for seep point data and synthetic data.

fold, and Shugg (2004) interprets that Tipperary Mineral Spring is located on the surface intersection of a thrust fault. Today, there is no clear evidence of this fault at outcrop. A borehole drilled in 2001 (for the handpump) is likely to have intersected this fault as indicated by the flow of gassy mineral water encountered at 45 m depth (Shugg, 2004). The flow of mineral waters carrying dissolved CO_2 from depth towards the surface may be guided by the geological structures such as the fault and/or the nearby anticline, similar to the hypothesis of Shugg (2009). The presence of ponded water in an otherwise dry creek during the dry season implies that mineral waters are seeping into the creek bed at the location of degassing. However, the mineral waters probably degas CO_2 during their ascent to surface; we observed dry seepage from outcropping rocks, while at nearby springs down-hole camera surveys found bubbles starting to form around 20–30 m below the water table (Shugg, 2009). When two-phase flow establishes, the CO_2 may migrate to surface via different pathways to its 'parent' water, depending on the hydraulic properties of the available flow pathways and water table depth. There is no appreciable thermal anomaly between the mineral waters and the surrounding groundwater (Weaver et al., 2006), so they are not ascending due to thermal buoyancy drive. Instead they may be migrating towards the surface due to a combination of hydraulic head and the fluid flow pathways offered by nearby structures, enhanced by buoyancy from gas lift due to CO_2 ebullition as the waters depressurise during ascent.

CO_2 seepage at Tipperary spring concentrates near the western sandstone-shale contact. Some 81% of total measured bubble stream emissions emerge from the shale dominated features in the river bed and we detected extremely localised dry seepage from open fractures

within outcropping sandstone and shale. The bedding and foliation orientation of rocks exposed in Sailors Creek follows the regional trend from NNW-SSE Devonian compression. Our spatial statistical analyses find that bubble point data exhibit this NNW-SSE (150-170°) trend at all point separation distances. Bubble points located within < 2 m of each other show other preferred alignments (NE-SW and SE-NW, NNE-SSW, ENE-WSW) but these trends are weak compared to the NNW orientations. Seepage mostly occurred in a narrow region, ~1 m width. In the field, we noted that bubble locations appeared to be primarily controlled by bedding and foliation planes, but also by fractures and joints across both the sandstone and shale members. Thus, while regional structures may govern mineral water and CO_2 flow (Shugg, 2009), it seems that primary features (the sandstone-shale contact) may control fluid flow in the deep and shallow subsurface, and at very shallow depths the small secondary structures (fractures, foliation) offer pathways to surface.

What is unusual at Tipperary is that gas primarily discharges from shales. Mudrocks and shales typically have low permeabilities, and high capillary entry pressures for two-phase flow, which makes them good seals for conventional hydrocarbon traps. At other sites around Daylesford, such as Sutton Spring, mineral water and gas discharges from the joints and fracture faces in sandstone beds (Shugg, 2009). These sandstones form the regional aquifer. Within these sandstone units intergranular porosity is limited to certain horizons. Therefore, groundwater flow is predominantly hosted by fractures and joints. Observations from exposed bedrock at Tipperary suggest that bulk rock permeability is most likely offered by the primary fracture set (NE-SW trend) together with the bedding. However, at Tipperary, our observations, corroborated by spatial statistical analyses, find that CO_2 bubbles preferentially emerge from foliation and fracture intersections in the shale. This indicates that in the shallow subsurface the high density of subvertical foliation and bedding-orthogonal fractures in the shale must be more transmissive than bedding and fracture planes in the sandstone. At outcrop, the fractured, folded and uplifted shales of the Ordovician succession clearly are not sealing. This could be due to unloading and weathering, and so these pathways have opened only close to the surface. Conversely, the bulk permeability of the shale units may be greater than the sandstone for these units. Fig. 6 schematically summarises the proposed mechanism for CO_2 delivery to the creek bed at Tipperary.

Other seeps worldwide emerge from clays. For example, in the Cheb Basin, CO_2 degassing close to a fault zone in clay dominated rocks occurs as highly localised emissions from fine fractures, facilitated by “micro-channels” in the clays which originated from shear (Bankwitz et al., 2003). Where low permeability rocks outcrop in Italy, CO_2 degassing occurs as vent like emissions rather than as springs or spring associated emissions, which more commonly occur from high permeability rocks (Roberts et al., 2014). However, at Tipperary, what is surprising is that CO_2 preferentially emerges from the shales rather than the sandstones.

That said, CO_2 seepage is not confined to the shale. Seepage occurs from sandstones submerged in Tipperary pool, and the CO_2 sniffer detected high CO_2 emissions from isolated points in the outcropping sandstone. Therefore there are gas flow pathways in the sandstone, but there are fewer pathways in the sandstone than in the shales (where gas emission is greater), and these pathways are extremely localised; occurring at jogs and intersections along low-dip bedding-orthogonal fractures, where they intersected the bedding plane (Fig. 5e).

Interestingly, the sniffer results indicate that it is likely that dry CO_2 seepage is greater from the outcropping sandstone than from outcropping shale. This is in contrast to CO_2 fluxes measured in Tipperary pool where more numerous and distributed bubble streams occur in the shale, and 75% of the total CO_2 flux via bubbles from Tipperary Pool is occurring from the shales. It is possible that this is a sampling artefact; the seep area is limited, the shale bed is thinner than the sandstones, and the area of outcrop is much smaller for the shale because it has preferentially eroded on the creek banks. If this is a real signal, there could be several explanations for the contrasting behaviour of the seeps through water and into air. Firstly, the rate of CO_2 seepage through the two lithologies could be the same but is occurring via distributed pathways (lots of small fractures and bedding partings) in the shale, with fewer localised high flux fracture-bedding intersections in the sandstone. As the shale was more foliated and thinly bedded, there were many more bedding parallel features to permit flow and so facilitate distributed seepage than in the massive bedded sandstone. Secondly, the outcrop style varies between the two lithologies: the sandstone stands proud of the surface and some individual bedding planes are exposed, whereas the shale is more eroded and the bedding is only viewed end-on. This means that the fractures that are low-dip (which are the ones that host the high dry seepage from the sandstone) are exposed in the sandstone, but are unlikely to be exposed in the shale at this site. Thirdly, flow pathways in the sandstone might be more likely to become obstructed by river sediments than the smaller aperture features in the shale. Regardless of the reason, our observations suggest that flow pathways in the very shallowest subsurface, and therefore how CO_2 seeps present, are highly sensitive to local conditions.

5.2. CO_2 flux at Tipperary

Estimating total CO_2 flux at Tipperary Spring is challenging given the intermittency of the CO_2 bubble streams. Bubbling, and therefore CO_2 flux, was not continuous in the pool. The flux of CO_2 from depth is probably continuous, but the bubbles are intermittent either due to high connectivity of the flow pathways (with flow paths turning ‘on’ and ‘off’) and/or due to water saturation of the flow pathways; CO_2 gas pressure must build enough to overcome capillary flow pressure, and the pressure of the water in the fracture. Such temporal and spatial variability has been observed at other CO_2 seeps including Laacher See (Germany $-CO_2$ bubbling is observed from the floor of a crater lake), Panarea (Italy - submarine geothermal region) and at the QICS project (Scotland - simulated CO_2 leak to the marine environment) Blackford et al. (2015) and Carammana pers. comm (2017). At a larger spatial scale, temporal and spatial variability in CO_2 emission has been observed at the Little Grand and Salt Wash faults in Utah over tens of thousands of years (Burnside et al., 2013). As such, intermittency of gas bubbling could be a universal phenomenon associated with gas flux into heterogeneous water-saturated media. This phenomenon is not restricted to CO_2. For example, the authors have observed intermittent bubbling of gases (predominantly nitrogen, but including CO_2, CH_4 and other short chain hydrocarbons) into creek beds in Northumberland (UK), and presumed to source from abandoned underground coal mines, which are common in this region.

Dynamic seepage has implications for strategies for sampling of natural gases, and also for estimating gas fluxes or total emissions. At Tipperary, the minimum total flux can be estimated from background diffuse degassing (79.2 g $m^{-2}d^{-1}$ or 4 kg y^{-1}), which does not include the contribution of individual bubbling seeps. Maximum flux can be estimated by assuming all measured bubble streams are active simultaneously, which equates to 116 g $m^{-2}d^{-1}$. However, since few bubble streams were active at the same time, this is an overestimate. In addition, our estimates do not consider dry CO_2 seepage from rocks by the pool, CO_2 dissolution (if the pool is not already saturated), or seasonal changes in the CO_2 emission.

Previous studies at natural CO_2 seeps find a range of CO_2 fluxes over several orders of magnitude, which poses challenges for the selection of appropriate monitoring devices and approaches. The rate of degassing depends on factors including soil and rock permeability, hydrogeological regime, and nature of the CO_2 source (Annunziatellis et al., 2008; Kirk, 2011). Fluxes at dry seeps such as mofettes can be very high e.g. 9000 g $m^{-2}d^{-1}$ at Florina (Greece) and 125,000 g m^{-2} d^{-1} in the Cheb Basin (Germany/Czech Republic) (Nickschick et al., 2015). But

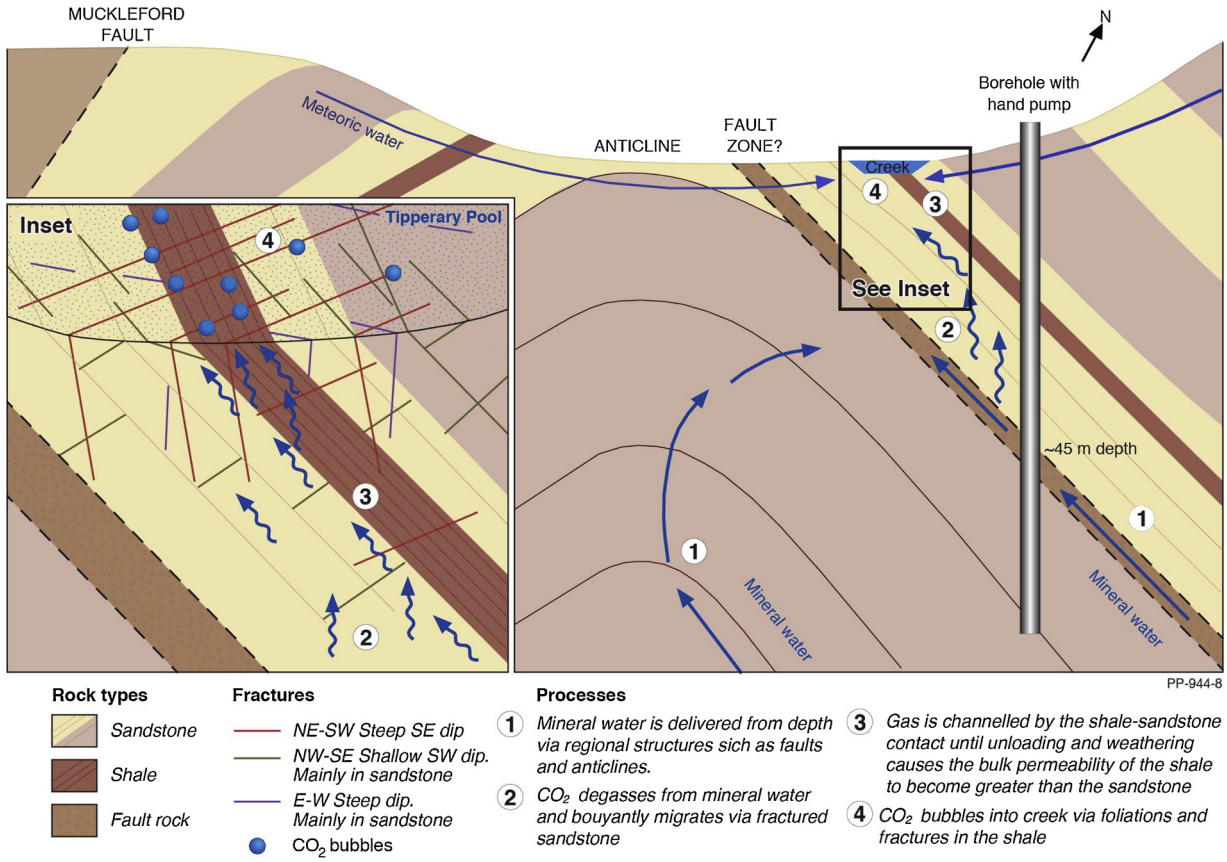

Fig. 6. Schematic 2D cross section (not to scale) of proposed model for CO_2 and mineral water flow pathways that give rise to Tipperary Mineral Spring and CO_2 seep. Inset: schematic 2.5D closeup of Tipperary Pool. While the shale may not be transmissive to fluids at depths where foliation and fractures are closed by overburden pressure, we propose that in the shallow subsurface unloading and weathering opens bedding, foliation and fractures enabling the shale to transmit fluids more readily than the fractured sandstone aquifer rocks. This causes the majority of CO_2 to be emitted via well-connected flow pathways in the shale unit in Tipperary Pool, and manifests as numerous and intermittent low flux bubble streams. CO_2 that is emitted straight to atmosphere ('dry seepage') is not intermittent. This implies that the turning 'on' and 'off' of bubble streams may result from capillary flow processes in the very shallow subsurface.

mofette systems are different from CO_2 degassing at mineral springs. Recent work at travertine bearing fault systems report fluxes that are more similar to Tipperary; maximum CO_2 fluxes were 191 g $m^{-2}d^{-1}$ at the Bongwana Fault (South Africa) (Bond et al., 2017) and calculated from travertine mass balance to be 1472 ± 677 and 18.8 ± 8.7 g $m^{-2}d^{-1}$ at two sites in Utah (USA) (Burnside et al., 2013).

Natural non-volcanic seeps are the most appropriate analogues for seeps that might potentially develop above engineered carbon stores, if injected CO_2 seeps to the surface by natural CO_2 pathways. However there are limitations to their comparability. Storage sites will be selected for specific sealing characteristics. In contrast, surface seepage at natural CO_2 seeps occur *because* the geology is not ideal for long term CO_2 trapping; the geology around Daylesford is composed of highly heterogeneous and tectonised sediments crossed by faults. Faulted reservoirs with heterogeneous or poorly permeable overburdens will probably not be selected for long term geological storage. In addition, natural CO_2 seeps will be migrating by natural fluid pathways whereas the greatest risks of CO_2 leakage from engineered CO_2 stores are man-made pathways, such as improperly sealed boreholes (IPCC, 2005) or geomechanical effects from the pressure response to CO_2 injection (Verdon et al., 2013). That said, natural CO_2 seeps may still be comparable to leakage through the overburden, independent of the leakage pathways from the reservoir, and seepage through clay formations, can serve analogues of CO_2 migration through cap rocks.

5.3. Implications for CCS

It is important to assure regulatory bodies and the public of CO_2 storage integrity. This includes demonstrating capability to (i) select storage sites that will successfully retain CO_2 in the subsurface, and (ii) identify potential CO_2 leakage and (iii) quantify any leaked CO_2.

In the case of CO_2 migration from onshore engineered storage sites, if the leaked CO_2 migrates to the near surface it could dissolve into groundwaters (and perhaps emerge as a dissolved constituent of groundwaters at natural springs), seep to atmosphere as a dry gas, or seep into water bodies such as lakes or rivers. Where migrating CO_2 dissolves into groundwaters, the groundwater flow systems will then govern its flow path, and only at shallow depth will decreasing pressures cause gas ebullition and facilitate the ascent of a separate gas phase. Indeed, studies of onshore natural analogues and field sites find that CO_2 seeps are more likely to emerge in topographic low points where there may be rivers or lakes, though there are examples of seeps that buck this trend (e.g. if flow is fault controlled) (Roberts et al., 2014).

In this work, we examine the surface expression of CO_2 seepage originating from transport of CO_2-rich regional groundwaters. We find that, while regional features may govern CO_2 delivery, in the shallow subsurface CO_2 pathways are localised to small scale geological features, and that fluxes are intermittent and consequently difficult to quantify due to the intermittency of bubbling pathways.

To date, most research has focussed on predicting the large-scale geological features that may enable CO_2 to migrate from the storage reservoir such as large faults, boreholes or gas chimneys (IEAGHG, 2017). Such macroscale (seismically resolvable) features are likely to be known about at the site characterisation phase of a project. However, shallow crustal processes change the rock properties that affect CO_2

spread and delivery to surface. Different, smaller scale geological features, that are not likely to be seismically resolvable, may become important controls on CO_2 flow in the shallow subsurface. At Tipperary, CO_2 seep distribution is controlled by microscale features such as foliation and bedding planes, joints and fractures in outcropping rock, probably dilated by uplift and weathering, which leads to degassing from a shale formation that is typically sealing. These observations support previous research investigating the role of topography and lithology in CO_2 seep location and characteristics (Roberts et al., 2014), and has important consequences for the design of CCS monitoring approaches. Surface monitoring programmes must focus on more than the processes and pathways governing leakage at depth; they must also consider how the CO_2 fluids leaked by natural or man-made pathways might disperse in the near surface and be expressed at the surface. These shallow processes will inform the design of the right monitoring tools and monitoring locations.

Our work thus provides insight into the scale of which geological features control CO_2 flow and the spatial and temporal variability of CO_2 leakage. Essentially, site characterisation during site selection and monitoring design must assess the geology and hydrogeology at a range of spatial scales. Surface processes, often overlooked, will govern the style and location of leakage, and so should inform the design of appropriate monitoring strategies.

6. Conclusions

We have studied the location and characteristics of CO_2 emission at Tipperary natural CO_2 seep in Daylesford, Victoria (Australia) as an analogue for leakage from engineered CO_2 stores. Seepage largely occurs as bubble streams in a pool in Sailors Creek, close to the Tipperary mineral springs which have high dissolved CO_2-content. We also observed CO_2 degassing from subaerial rock outcrop. Observation and spatial statistical analyses find that at a meso-scale (multiple meters) the location of CO_2 bubble streams are controlled by the sandstone-shale geological contact. At a smaller (meter to centimetre) scale, gas emission is controlled by structural features, primarily fractures intersecting the foliation or bedding planes. The intermittency of the bubble streams, and their distribution, makes CO_2 flux challenging to quantify. Unusually, CO_2 emission is greatest from the shale, rather than the sandstone that forms the regional aquifer. Surface processes are likely to be affecting rock transmissivity, which governs CO_2 flow at the near surface. Our work has important implications for characterising and monitoring of CO_2 stores: microscale features and near surface processes can have significant effect on CO_2 leak locations and rates. Flow pathways through the very shallowest part of the subsurface are highly dependent on local conditions, and may produce the highest flux in counter-intuitive locations (e.g. hosted by the 'low permeability' shales at Tipperary). Understanding of shallow crustal processes and specific site conditions are essential to inform the design of effective surface monitoring tools and approaches. Secondly, should leakage from the storage reservoir occur, the surface leak identification and quantitation approaches must be extended to consider intermittent or variable CO_2 emission rates.

Data availability statement

All data (precise bubble locations and distributions, fluxes, and whether bubbling occurred at a fracture or foliation/bedding at Tipperary pool), are available from the UKCCSRC Data and Information Archive, under the DOI: (to be added).

Acknowledgements

We are grateful for contributions, discussions, and assistance from Jade Anderson, Ivan Schroder and Tim Evans (Geoscience Australia), Giorgio Caramanna (GeoAqua Consulting), Anthony Handley (Parks Victoria), and Andy Shugg. We thank Bart Thomas, Ryan Ruddick and Auscope for providing RTK equipment and training and Suman George (University of Western Australia/National Geosequestration Laboratory) for providing the Li−COR 81,000 A soil gas flux system. Many thanks to David Arnold (Geoscience Australia) for his help preparing the illustrations in this paper. We also thank Sabina Bigi and her team at Sapienza Università di Roma for providing information on the composition of gases observed bubbling into streams in Northumberland in 2017.

The authors would like to acknowledge the financial support of the UK CCS Research Centre (www.ukccsrc.ac.uk) in carrying out this work (grant number UKCCSRC-C1-31). The UKCCSRC is funded by the EPSRC (EP/K000446/1, EP/P026214/1) as part of the RCUK Energy Programme. We also thank the UKCCSRC, University of Strathclyde, CSIRO and Geoscience Australia for supporting this work through Roberts' International Research Collaboration Fund. Our collaborative fieldwork in Northumberland with Sapienza Università di Roma was supported by the University of Strathclyde and the EU-funded ENOS project (H2020-EU.3.3.2.3; grant no. 653,718).

Annex A Accumulator chamber factor for CO_2 flux measurements

To convert the rate of change in CO_2 concentration measured in the accumulation change (e.g. in ppm/s) to a flux (mole/m^2/day), the rate needs to be multiplied by a correction factor which considers the volume of the chamber, temperature and pressure:

$$K = \frac{86400 \bullet P}{10^6 \bullet R \bullet T_k} \bullet \frac{V}{A}$$

where

- P is the barometric pressure expressed in mBar
- R is the gas constant 0.0831451 bar K^{-1} mol^{-1}
- T_k is the air temperature expressed in degrees Kelvin
- V is the chamber net volume in cubic meters (less the portion of the chamber submerged to create a seal on the water surface)
- A is the chamber inlet area in square meters

References

Annunziatellis, A., Beaubien, S.E., Bigi, S., Ciotoli, G., Coltella, M., Lombardi, S., 2008. Gas migration along fault systems and through the vadose zone in the Latera caldera (central Italy): implications for CO2 geological storage. Int. J. Greenh. Gas Control. 2 (3), 353–372.

Bankwitz, P., Schneider, G., Kämpf, H., Bankwitz, E., 2003. Structural characteristics of epicentral areas in Central Europe: study case Cheb Basin (Czech Republic). J. Geodyn. 35 (1), 5–32.

Blackford, J., Bull, J.M., Cevatoglu, M., Connelly, D., Hauton, C., James, R.H., Lichtschlag, A., Stahl, H., Widdicombe, S., Wright, I.C., 2015. Marine baseline and monitoring strategies for carbon dioxide capture and storage (CCS). Int. J. Greenh. Gas Control. 38, 221–229.

Bond, C.E., Wightman, R., Ringrose, P.S., 2013. The influence of fracture anisotropy on CO 2flow. Geophys. Res. Lett. 40, 1284–1289. https://doi.org/10.1002/grl.50313.
Bond, C.E., Kremer, Y., Johnson, G., Hicks, N., Lister, R., Jones, D.G., Haszeldine, R.S., Saunders, I., Gilfillan, S.M.V., Shipton, Z.K., Pearce, J., 2017. The physical characteristics of a CO2 seeping fault: the implications of fracture permeability for carbon capture and storage integrity. Int. J. Greenh. Gas Control 61, 49–60. https://doi.org/10.1016/j.ijggc.2017.01.015.
Bonnet, E., Bour, O., Odling, N.E., Davy, P., Main, I., Cowie, P., Berkowitz, B., 2001. Scaling of fracture systems in geological media. Rev. Geophys. 39 (3), 347–383. https://doi.org/10.1029/1999RG000074.
Burnside, N.M., Shipton, Z.K., Dockrill, B., Ellam, R.M., 2013. Man-made versus natural CO2 leakage: a 400 k.y. History of an analogue for engineered geological storage of CO2. Geology 41 (4), 471–474. https://doi.org/10.1130/G33738.1.
Carpenter, M., Kvien, K., Aarnes, J., 2011. The CO2QUALSTORE guideline for selection, characterisation and qualification of sites and projects for geological storage of CO2. Int. J. Greenh. Gas Control 5 (4), 942–951. https://doi.org/10.1016/j.ijggc.2010.12.005.
Cartwright, I., Weaver, T., Tweed, S., Ahearne, D., 2000. O, H, C isotope geochemistry of carbonated mineral springs in central Victoria, Australia: sources of gas and water–rock interaction during dying basaltic volcanism. J. Geochem. Exp. 69-70, 257–261. https://doi.org/10.1016/s0375-6742(00)00059-5.
Cartwright, I., Weaver, T., Tweed, S., Ahearne, D., 2002. Stable isotope geochemistry of cold CO 2-bearing mineral spring waters, Daylesford, Victoria, Australia: sources of gas and water and links with waning volcanism. Chem. Geol. 185 (1), 71–89. https://doi.org/10.1016/S0009-2541(01)00397-7.
Chiodini, G., Frondini, F., Cardellini, C., Granieri, D., Marini, L., Ventura, G., 2001. CO2 degassing and energy release at Solfatara volcano, Campi Flegrei, Italy. J. Geophys. Res. 106, 16213–16221. https://doi.org/10.1029/2001jb000246.
Cox, S.F., Etheridge, M.A., Cas, R., 1991a. Deformational style of the Castlemaine area, Bendigo-Ballarat Zone: Implications for evolution of crustal structure in central Victoria. Aust. J. Earth Sci. 38, 151–170. https://doi.org/10.1080/08120099108727963.
Cox, S.F., Wall, V.J., Etheridge, M.A., Potter, T.F., 1991b. Deformational and metamorphic processes in the formation of mesothermal vein-hosted gold deposits—examples from the Lachlan Fold Belt in central Victoria, Australia. Ore Geol. Rev. 6, 391–423.
Dixon, T., McCoy, S.T., Havercroft, I., 2015. Legal and regulatory developments on CCS. Int. J. Greenh. Gas Control 40, 431–448. https://doi.org/10.1016/j.ijggc.2015.05.024.
Dockrill, B., Shipton, Z.K., 2010. Structural controls on leakage from a natural CO2 geologic storage site: central Utah, U.S.A. J. Struct. Geol. 32 (11), 1768–1782. https://doi.org/10.1016/j.jsg.2010.01.007.
Faulkner, D.R., Jackson, C.A.L., Lunn, R.J., Schlische, R.W., Shipton, Z.K., Wibberley, C.A.J., Withjack, M.O., 2010. A review of recent developments concerning the structure, mechanics and fluid flow properties of fault zones. J. Struct. Geol. 32 (11), 1557–1575. https://doi.org/10.1016/j.jsg.2010.06.009.
Feitz, A.J., Leamon, G., Jenkins, C., Jones, D.G., Moreira, A., Bressan, L., Melo, C., Dobeck, L.M., Repasky, K., Spangler, L.H., 2014. Looking for leakage or monitoring for public assurance? Energy Procedia 63, 3881–3890. https://doi.org/10.1016/j.egypro.2014.11.418.
Gill, E.D., 1964. Rocks contiguous with the basaltic cuirass of Western Victoria. Proc. R. Soc. Vic. 77, 331–355.
Gray, D.R., Willman, C.E., 1991. Deformation in the Ballarat Slate Belt, central Victoria, and implications for the crustal structure across southeast Australia. Aust. J. Earth Sci. 38, 171–201. https://doi.org/10.1080/08120099108727964.
Gray, D.R., Wilson, C.J.L., Barton, T.J., 1991. Intracrustal detachments and implications for crustal evolution within the Lachlan fold belt, southeastern Australia. Geology 19 (6), 574–577. https://doi.org/10.1130/0091-7613(1991)019<0574:IDAIFC>2.3.CO;2.
Hippler, S.J., 1993. Deformation microstructures and diagenesis in sandstone adjacent to an extensional fault: implications for the flow and entrapment of hydrocarbons. AAPG Bull. 77, 625–637.
Holloway, S., Pearce, J.M., Hards, V.L., Ohsumi, T., Gale, J., 2007. Natural emissions of CO2 from the geosphere and their bearing on the geological storage of carbon dioxide. Energy 32 (7), 1194–1201. https://doi.org/10.1016/j.energy.2006.09.001.
IEAGHG, 2017. CO2 Migration in the Overburden. IEAGHG Technical Reports. IEA Greenhouse Gas R&D Programme.
IPCC, 2005. IPCC Special Report on Carbon Dioxide Capture and Storage. Prepared by Working Group III of the Intergovernmental Panel on Climate Change.
Jenkins, C., Chadwick, A., Hovorka, S.D., 2015. The state of the art in monitoring and verification—ten years on. Int. J. Greenh. Gas Control 40, 312–349. https://doi.org/10.1016/j.ijggc.2015.05.009.
Karolytė, R., Serno, S., Johnson, G., Gilfillan, S.M.V., 2017. The influence of oxygen isotope exchange between CO2 and H2O in natural CO2-rich spring waters: implications for geothermometry. Appl. Geochem. 84, 173–186. https://doi.org/10.1016/j.apgeochem.2017.06.012.
Kirk, K., 2011. Natural CO2 Flux Literature Review for the QICS Project (No. CR/11/005). British Geological Survey Commissioned Report.
Laing, A.C.M., 1977. Daylesford – Hepburn Springs Mineral Water Investigation. Dept. of Minerals and Energy and the Geological Survey of Victoria, Melbourne.
Lawrence, C.R., 1969. Hydrogeology of the Daylesford District with Special Reference to the Mineral Springs 1–40. Dept. of Mines, Geological Survey, Melbourne.
Maddicks, H.T., Butler, K.H., 1981. 100 Years of Daylesford Gold Mining History. Daylesford Historical Society, Victoria.
McCay, A.T., Shipton, Z.K., Lunn, R.J., Gale, J.F., 2018. Mini Thief Zones: Sub-centimeter Sedimentary Features Enhance Fracture Connectivity in Shales. Bulletin of the American Association of Petroleum Geologistshttps://doi.org/10.1306/0918181610617114.
Mcdougall, I., Allsop, H.L., Chamalaun, F.H., 1966. Isotopic dating of the newer volcanics of Victoria, australia, and geomagnetic polarity epochs. J. Geophys. Res. 71, 6107–6118. https://doi.org/10.1029/JZ071i024p06107.
Miocic, J.M., Gilfillan, S.M.V., Roberts, J.J., Edlmann, K., McDermott, C.I., Haszeldine, R.S., 2016. Controls on CO 2 storage security in natural reservoirs and implications for CO 2 storage site selection. Int. J. Greenh. Gas Control 51, 118–125. https://doi.org/10.1016/j.ijggc.2016.05.019.
Nickschick, T., Kämpf, H., Flechsig, C., Mrlina, J., Heinicke, J., 2015. CO2 degassing in the hartoušov mofette area, western eger rift, imaged by CO2 mapping and geoelectrical and gravity surveys. Int. J. Earth Sci. 104, 2107–2129.
OECD/IEA, 2015. Carbon Capture and Storage: the Solution for Deep Emissions Reductions. IEA Publishing.
Oldenburg, C.M., Lewicki, J.L., 2006. On leakage and seepage of CO2 from geologic storage sites into surface water. Environ. Geol. 50 (5), 691–705. https://doi.org/10.1007/s00254-006-0242-0.
Osborne, C., Bibby, L., Willman, C., Maher, S., Hollis, J., 2002. Daylesford 1:50 000 Geological Map. Geological Survey of Victoria.
Pearce, J., Czernichowski-Lauriol, I., 2004. A review of natural CO2 accumulations in Europe as analogues for geological sequestration. Geol. Soc. London Spec. Pub. 233, 29–41. https://doi.org/10.1144/GSL.SP.2004.233.01.04.
Richards, J.R., Singleton, O.P., 1981. Palaeozoic Victoria, Australia: igneous rocks, ages and their interpretation. J. Geol. Soc. Aust. 28, 395–421. https://doi.org/10.1080/00167618108729178.
Rinaldi, A.P., Rutqvist, J., 2013. Modeling of deep fracture zone opening and transient ground surface uplift at KB-502 CO2 injection well, in Salah, Algeria. Int. J. Greenh. Gas Control 12, 155–167. https://doi.org/10.1016/j.ijggc.2012.10.017.
Roberts, J.J., Stalker, L., 2017. What have We Learned about CO2 Leakage from Field Injection Tests? Energy Procedia 114 (Supplement C), 5711–5731.
Roberts, J.J., Wood, R.A., Wilkinson, M., Haszeldine, S., 2014. Surface controls on the characteristics of natural CO2 seeps: implications for engineered CO2 stores. Geofluids 15, 453–463. https://doi.org/10.1111/gfl.12121.
Roberts, J.J., Wilkinson, M., Naylor, M., Shipton, Z.K., Wood, R.A., Haszeldine, R.S., 2017a. Natural CO2 sites in Italy show the importance of overburden geopressure, fractures and faults for CO2 storage performance and risk management. Geol. Soc. London Spec. Pub. 458, 181–211. https://doi.org/10.1144/SP458.14.
Roberts, J.J., Gilfillan, S.M.V., Stalker, L., Naylor, M., 2017b. Geochemical tracers for monitoring offshore CO2 store. Int. J. Greenh. Gas Control 65, 218–234. https://doi.org/10.1016/j.ijggc.2017.07.021.
Roberts, J.J., Feitz, A.J., Leplastrier, A., Anderson, J., Schroder, I., 2019. Quantifying CO2 leak rates in aquatic environments (in press). SSRN: GHGT-14 Proceedings.
Schaffer, M., Maier, F., Licha, T., Sauter, M., 2013. A new generation of tracers for the characterization of interfacial areas during supercritical carbon dioxide injections into deep saline aquifers: kinetic interface-sensitive tracers (KIS tracer). Int. J. Greenh. Gas Control 14, 200–208. https://doi.org/10.1016/j.ijggc.2013.01.020.
Shugg, A., 1996. Mineral and Spring Water Resource Protection Discussion Paper. Department of Natural Resources and Environment, Melbourne.
Shugg, A., 2004. Sustainable Management of the Central Victorian Mineral Waters. PhD, RMIT University, Melbourne.
Shugg, A., 2009. Hepburn spa: cold carbonated mineral waters of Central Victoria, south Eastern Australia. Environ. Geol. 58, 1663–1673. https://doi.org/10.1007/s00254-008-1610-8.
Shugg, A., Brumley, J.C., 2003. Environmental, hydrogeological and conflict as elements determining the long term viable development of carbonated mineral waters of hepburn, Victoria. In Proc. Nation. Env. Conf. Brisbane.
VandenBerg, A., 1978. The Tasman fold belt system in Victoria. Tectonophysics 48, 159–205. https://doi.org/10.1016/0040-1951(78)90118-x.
Verdon, J.P., Kendall, J.-M., Stork, A.L., Chadwick, R.A., White, D.J., Bissell, R.C., 2013. Comparison of geomechanical deformation induced by megatonne-scale CO2 storage at Sleipner, Weyburn, and in Salah. Proc. Nat. Acad. Sci. 110 (30), E2762–E2771. https://doi.org/10.1073/pnas.1302156110.
Vollmer, F.W., 2015. Orient 3: a new integrated software program for orientation data analysis, kinematic analysis, spherical projections, and Schmidt plots. Geol. Soc. Am. 47 (7), 49 Abstracts with Programs.
Weatherzone, 2017. Ballarat Ap Observations. Accessed on 02/08/17. http://www.weatherzone.com.au/station.jsp?lt=site&lc=89002&list=ob.
Weaver, T.R., Cartwright, I., Tweed, S.O., Ahearne, D., Cooper, M., Czapnik, K., Tranter, J., 2006. Controls on chemistry during fracture-hosted flow of cold CO2-bearing mineral waters, Daylesford, Victoria, australia: implications for resource protection. Appl. Geochem. 21, 289–304. https://doi.org/10.1016/j.apgeochem.2005.09.011.
Wishart, E., Wishart, M., 1990. The Spa Country: a Field Guide to 65 Mineral Springs of the Central Highlands, Victoria. Spa Publishing, Daylesford.